Asian Journal of Chemistry; Vol. 32, No. 9 (2020), 2213-2221

ASIAN JOURNAL OF CHEMISTRY

https://doi.org/10.14233/ajchem.2020.22750

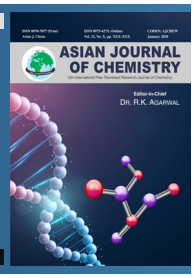

Synthesis, Spectral Characterization, Crystal Structure, Thermal Studies and Hirshfeld Surface Analysis of Novel Dichlorodi-(*E*)-*N*′-(4-methoxybenzylidene)benzohydrazide Manganese(II) Complex

G. Kavitha[1], M. Uthayakumar[2], Vandana Shinde[3,], T. Chandrasekaran[4] and M. Suresh[5,*,]

[1]Department of Chemistry, Rajalakshmi Institute of Technology, Kuthambakkam, Chennai-600124, India
[2]Department of Physics, Jayarani Arts and Science college for Women, Salem-636002, India
[3]Department of Physics, Kavayitri Bahinabai Chaudhari North Maharashtra University, Jalgaon-425001, India
[4]Sir Sivaswamy Iyer Higher Secondary School, Thirukattupalli, Thanjavur-613104, India
[5]Department of Chemistry, Pachaiyappa's College for Men, Kanchipuram-631501, India

*Corresponding author: E-mail: mscsuresh2@gmail.com

Received: 31 March 2020; *Accepted*: 27 May 2020; *Published online*: 20 August 2020; AJC-20015

A novel dichlorodi(*E*)-*N*′-(4-methoxybenzylidene)benzohydrazide manganese(II) (ENMB-Mn) complex has been successfully synthesized using (*E*)-*N*′-(4-methoxybenzylidene)benzohydrazide (ENMB) as ligand. The structure of the ENMB-Mn complex was studied by single crystal X-ray diffraction, UV-Visible, FTIR, thermogravimetric analysis (TGA) and Hirshfeld surface analysis. Results of single crystal X-ray diffraction found that the structure of ENMB-Mn complex crystal is triclinic with space group P-1 and lattice parameters of unit cell a, b and c values were 7.1900 Å, 8.9094 Å and 11.8130 Å, respectively. The structure of ENMB-Mn complex clearly indicates complete octahedral geometry $[Mn(ENMB)_2Cl_2]$ with manganese(II) ion, where the ENMB and chlorine atoms ratio is 1:2:2, respectively. Further, the molecular properties like Hirshfeld surface analysis mapping are reported.

Keywords: Benzohydrazide manganese(II) complex, Schiff base, Single crystal XRD, Hirshfeld surface analysis.

INTRODUCTION

The label 'Schiff base' contains two words, the first word represents the name of German chemist Hugo Schiff, who has synthesized Schiff base for the first time and second word indicates its base type nature [1]. These types of compounds have wide range of applications from biological to electronics [2]. Condensation reactions between ketone or aldehyde with primary amines resulting the Schiff base compounds.

In order to develop new coordination compounds, various research groups have tried to synthesis of Schiff base ligands using transition metals which results outstanding and tunable properties related to stereo-electronic structure [3]. Such kind of new compounds are highly useful in various fields like gas sensors, catalysis, electroluminescence, photoluminescence, drug delivery and membranes [4-16]. Therefore numerous researchers are motivated towards these types of compounds. In last two-three decades, symmetrically-substituted Schiff base with co-centered metal complexes are the interest of research since they possess important superior catalytic behaviour, biological activities and second order non-linear optical properties, *etc*. The purpose of metal incorporation in structure is similar to metal organic frameworks such as metal centers and organic linkers, which have remarkable capability to dominate and alter their properties superior way like gas sorption/separation, water sorption/desorption, proton conductivity and drug delivery [17,18]. In this way, symmetrical and unsymmetrical Schiff bases contributing the progress in coordination chemistry of transition metals and major group elements.

The significant characteristic of these materials are they show the "breathing effect" which means it capture metal cations as host in organic frameworks and it have flexible periodic structure which shows deformation in structure by external agency. Therefore, it is used for wide range of applications, which make these compounds as a versatile [19,20]. In brief, Shakdofa *et al*. [21] reported a review article on the metal complexes of

hydrazones with the variety of applications. Hosseini-Monfareda *et al*. [22] reported the synthesis of ONN and ONO hydrazone Schiff base ligands. Further their crystal structure and catalytic activity of complexation with manganese metal ion also investigated. Rathi *et al*. [23] also reported the synthesis of few Mn(II) complexes of tridentate NNN donor ligands and their DNA interaction, nuclease and protease activities are explained. The Mn(II) triazamacrocyclic complexes synthesized and its structural, spectroscopic, electrochemical and magnetic properties have been investigated by Banerjee *et al*. [24].

In recent years, several works reported the hydrolysis of phosphoric and carboxyl esters based Schiff bases and their applications in the field of environment and biological fields are also analyzed [25]. Variety of metals incorporated Schiff bases catalysts are found in literature but Mn(II) and Co(II) incorporated catalysts are the cost effective and more effective catalysts species in hydrolysis of phosphoric and carboxyl esters [26,27]. The synthesis and characterization of four Mn(II) and Co(II) complexes incorporated by unsymmetrically substituted tetradentate Schiff base ligands are also reported by Li *et al*. [28]. These complexes have excellent catalytic activities for hydrolysis reactions. They observed that with increase in pH, the reaction rate also increased. Shaabani *et al*. [29] studied antimicrobial behaviour and crystal structure of hydrazone Schiff base and azide ligands incorporated by Cr(III), Mn(II) and Fe(III). Boutar *et al*. [30] also reported Zn(II) and Mn(II) incorporated calix[4]arene functionalized with carboxylates complexation.

The literature survey indicates that the synthesis, characterization including single crystal XRD (SCXRD) and Hirshfield studies have not been documented of the title compound so far. The present work reports the synthesis of manganese(II) complex of (*E*)-*N*′-(4-methoxybenzylidene)benzohydrazide (ENMB-Mn) and characterized by FTIR, UV-Visible absorption spectroscopy, SCXRD analysis. The structure of ENMB ligand is evaluated using FTIR, UV-visible, ^{1}H & ^{13}C NMR and mass spectral studies. The thermal properties and intramolecular interaction of title compound also studied by TGA and Hirshfeld surface analysis.

EXPERIMENTAL

A.R. grade anisaldehyde, benzohydrazide, hydrochloric acid, manganese(II) chloride, ethanol and ether were purchased from Merck and Sigma-Aldrich suppliers and used without any purification. Analytical TLC was carried on silica coated glass plates.

Synthesis of dichlorodi(*E*)-N′-(4-methoxybenzylidene)-benzohydrazide (ENMB) ligand: Initially, an ethanolic solution of anisaldehyde (3.4 mL, 0.025 mol) was measured in flask, after then benzohydrazide (3.4 g, 0.025 mol) and a little drops of hydrochloric acid were mixed into the solution. This reaction mixture was stirred well keeping in an ice bath for 3 h. After completion of the reaction that was checked by TLC. The colourless solid formed was filtered, washed several times with petroleum ether (40-60%).The crude solid ENMB ligand, thus obtained was dried over in vacuum and recrystallized using ethanol (**Scheme-I**).

Synthesis of ENMB-Mn complex: Ethanolic solution of ENMB ligand (2.15 g, 0.01 mol) and manganese(II) chloride (0.85 g, 0.005 mol) were mixed in flask. This reaction mixture kept stirring and refluxed at 85 ºC for 8 h. Then after, solution kept stable for three days at room temperature. On the fourth day, a pale violet coloured crystalline solid of ENMB-Mn was observed. The product solution was filtered from the reaction mixture, washed several times with petroleum ether and dried at room temperature. The product was recrystallized using ethanol and dried in vacuum (**Scheme-II**).

Characterization: FTIR spectra were recorded in the frequency range of 4000-400 cm^{-1} using Shimadzu FTIR 400 spectrophotometer, by KBr pellet technique. The UV-Visible absorption spectra were measured using Perkin-Elmer Lambda 35 model spectrophotometer in the wavelength range 190-1100 nm. ^{1}H & ^{13}C NMR spectra of samples were recorded at 300 MHz and 100 MHz, respectively using DMSO-d_6 as solvent

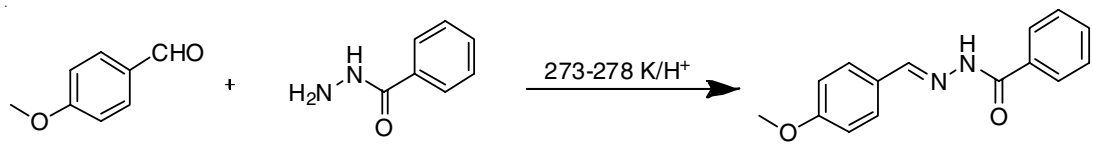

Scheme-I: Synthesis of ENMB ligand

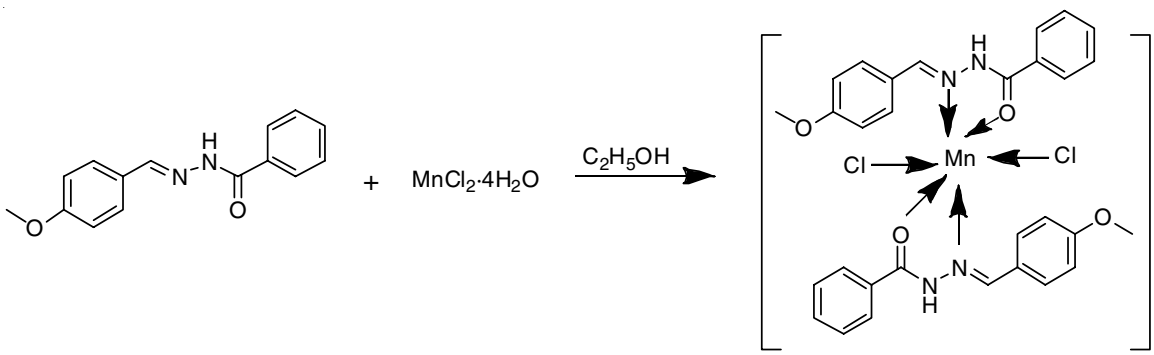

Scheme-II: Synthesis of ENMB-Mn complex

at room temperature by Bruker NMR Spectrometer. A mass spectrum was measured by using JEOL mass spectrometer, operating at an ionization potential of 70 eV. Bruker Kappa diffractometer with X-ray source Mo (wavelength of Kα line = 0.71073 Å) using in the ω/2θ scan mode at room temperature was used to collect the crystal structure data of ENMB-Mn crystal. The thermal behaviour of ENMB-Mn complex was studied by TGA using thermogravimetric analyzer TGA 4000-Perkin-Elmer model temperature varied from room temperature to 900 ºC keeping a heating rate of 15 ºC/min in a nitrogen atmosphere. The Hirshfeld surfaces of ENMB-Mn crystal were generated using Crystal Explorer 3.1 software using the Crystallography Informative File (CIF) [31].

RESULTS AND DISCUSSION

FT-IR studies: FTIR spectra of ENMB and ENMB-Mn complex are shown in Fig. 1. The band appeared at 1668 cm^{-1} indicates the ν(-C=N) stretching of azomethine moiety of the ENMB ligand. This band observed to be shifted to the lower frequency in the manganese complex (ENMB-Mn) at 1645 cm^{-1} by nearly 23 cm^{-1}. This suggests that the coordination is observed through N-atom of azomethine (-CH=N-) linkage [12]. The carbonyl group (C=O) stretching frequency of ENMB ligand was observed at 1675 cm^{-1} while the same was observed at 1678 cm^{-1} for ENMB-Mn complex, which suggests the oxygen atom included in carbonyl group of ligand bounds with Mn(II) ions. The amide group in ligand exhibits a peaks at 3322 and 3150 cm^{-1}, which corresponds to NH symmetric and asymmetric stretching modes, respectively, while ENMB-Mn complex has been found stretching bands at 3325 and 3152 cm^{-1}, which indicates that there is absence of nitrogen atom of amide group in ligand binding with Mn(II) ions [32-34]. The bands for CH, C=C stretching, NH bending modes and other modes are not having considerable change in the both complex and ligand. The assigned values are given in Table-1 [35-40].

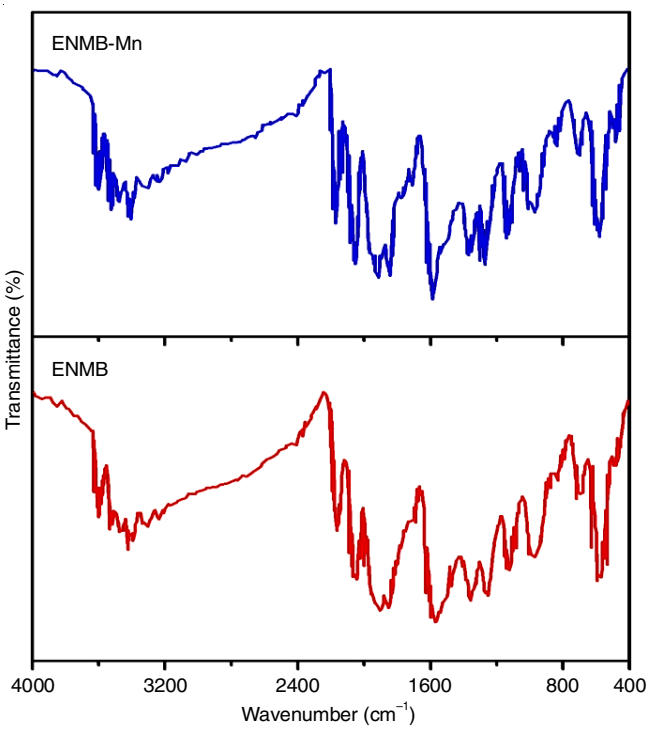

Fig. 1. FT-IR spectrum of ENMB and ENMB-Mn complex

TABLE-1
FT-IR ASSIGNMENTS FOR LIGAND (ENMB) AND ITS TITLE COMPOUND (ENMB-Mn)

Frequency (ν, cm^{-1})		Assignments
ENMB	ENMB-Mn	
3430	3422	N-H symmetric stretching
2902.55	2902.70	Aromatic C-H stretching
2846.58	2846.50	Aliphatic CH stretching
1675.64	1678.12	C=O stretching
1594.78	1592.84	NH bending
1492.53, 1447.95	1492.62, 1445.94	C=C bending
1249.62	1255.50	C=N stretching
–	459.24	Mn-N bending
–	409.38	Mn-Cl bending

UV-visible studies: The UV-visible spectra of ENMB and ENMB-Mn are shown in Fig. 2. The broad peak with small absorbance observed at 206 nm indicates that high energy π-π* transitions. This peak suggesting that the presence of delocalization of π electron from the benzene rings of ligand ENMB. An another one peak observed at 230 nm, arises due to n-σ* transition indicating that the non-bonding electrons on nitrogen atom in amines are loosely bound as compared to n-electrons on oxygen atom in the ligand ENMB.

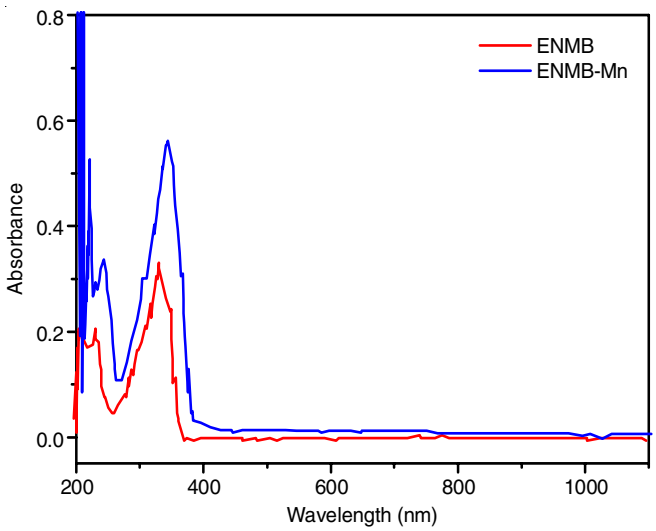

Fig. 2. UV-visible spectrum of ligand ENMB and ENMB-Mn complex

In the coordination compound, the maximum absorption band is ascertained to be at 329 nm, which may arise due to n→π* transition corresponds to the promotion of an electron from a bonding orbital to an antibonding π* orbital available in ligand compound with unsaturated centers. While on the other hand, UV-visible spectrum of ENMB-Mn shows the maximum absorption band at 343 nm, which may arise due to n→π* transition corresponds originated from the ligand metal charge transfer (LMCT) interactions. In the coordination compound, the maximum absorption band is ascertained to be at 243 nm, which may arise due to n→π* transitions [41,42].

NMR studies: The ^{1}H NMR spectrum of ENMB ligand shows a singlet 11.8 ppm with their characteristic proton couplings indicate the presence of amide protons (CONH), but it exist keto-enolic tautomer form in DMSO-d_6 solvent. The ^{1}H NMR chemical shift at 8.4 ppm with sharp singlet indicates the presence of azomethine proton (CH=N). One doublet is appeared at δ 7.9 ppm which corresponds to two aromatic *ortho*-CH proton of phenyl ring of benzohydrazide part. Doublet signals appeared at δ 7.7 ppm and 7.0 ppm corresponds to four aromatic CH protons of aldehyde part of the compound. Two triplets appeared at about δ 7.6 and 7.5 ppm indicating three aromatic CH protons of the *para* and *meta*-position of benzo-hydrazide phenyl ring. Further one sharp singlet peak at δ 3.8 ppm suggesting the methyl protons of the ligand.

The results of ^{13}C NMR of ENMB ligand analysis provide information regarding the twelve peaks of the carbon atom with different electronic environments. The signal appears at the chemical shift (δ) 168 ppm is correspond to carbonyl carbon and the signals exhibit at δ 163, 148, 137, 129, 128, 127 and 114 ppm are attributed to benzene ring carbons of both anisaldehyde and benzohydrazide part. A peak signal appeared at δ 152 ppm, which is corresponding to azomethine carbon. At lower chemical shift 57 ppm one more signal observed which indicates carbon of methoxy group [43,44].

Mass studies: Mass spectrum of ENMB ligand was recorded by electron ionization method and its fragmentation pattern is shown in **Scheme-III**. The calculated molecular weight of the synthesized ENMB ligand is 254 and the mass spectrum also displays a peak at *m/z* 254, which supports the synthesized ENMB ligand ($C_{16}H_{14}N_2O_4$(I)). Further, a peak appears at *m/z* 148, which is due to the structure $C_8H_8N_2O$ (II). And a peak at *m/z* 133 is corresponds to the fragment of $C_7H_5N_2O^+$ ion (III). A peak with high intensity appears at *m/z* 105 corresponds to $C_7H_5O^+$ ion (IV) which is known as base peak and further it will disintegrate to give two peaks at *m/z* 91 and 77 which is due to the $C_7H_7^+$ (V) and $C_7H_5^+$ (VI) ions, respectively. Thus mass spectrum clearly shows the formation of ENMB ligand *via* various intermediate cations, which will finally results to the stable ligand.

Single crystal XRD study of ENMB-Mn: The single crystal XRD has been carried out to investigate structure and the lattice parameter for the grown ENMB-Mn crystal. The collected crystal structural data of ENMB-Mn was deposited in Cambridge Crystallographic Data Centre (CCDC) with CCDC number is 1901365. The lattice parameters of ENMB-Mn crystal are a = 7.1900(4) Å, b=8.9094(5) Å, c = 11.8130(7) Å and volume V = 721.21(7) Å^3 . The minimum and maximum value of residual electron density was -0.351 and 0.338e Å^{-3} respectively and the final R-factor were 0.0430. The full-matrix least squares refinement results are given in Table-2. The some selected bond lengths and bond angles are shown in Tables 3 and 4, respectively. The solved final molecular structure (ORTEP) and crystal packing diagram with hydrogen bonding interaction of grown ENMB-Mn crystal are shown in Figs. 3 and 4.

The ENMB-Mn crystal belongs to the triclinic system corresponding from the space group P-1, which is recognized

TABLE-2
CRYSTALLOGRAPHIC DATA OF THE ENMB-Mn COMPOUND

Empirical formula	$C_{30}H_{28}N_4O_4Cl_2Mn$
Formula weight	634.40
Temperature	296(2) K
Wavelength	0.71073 Å
Crystal system, space group	Triclinic, P-1
Unit cell dimensions	a = 7.1900(4) Å α = 94.064(4)°
	b = 8.9094(5) Å β = 101.718(3)°
	c = 11.8130(7) Å γ = 101.485(3)°
Volume	721.21(7) Å^3
Z, Calculated density	2, 1.461 Mg/m^3
Absorption coefficient	0.686 mm^{-1}
F(000)	327
Crystal size	0.35 × 0.30 × 0.25 mm
Theta range for data collection	1.77 to 28.27°
Limiting indices	-9<=h<=9, -11<=k<=11, -15<=l<=15
Reflections collected / unique	5620 / 3421 [R(int) = 0.0140]
Completeness to theta = 28.27	95.4%
Absorption correction	Semi-empirical from equivalents
Max. and min. transmission	0.8472 and 0.7953
Refinement method	Full-matrix least-squares on F^2
Data / restraints / parameters	3421 / 0 / 195
Goodness-of-fit on F^2	1.129
Final R indices [I>2σ(I)]	R1 = 0.0314, wR2 = 0.0912
R indices (all data)	R1 = 0.0430, wR2 = 0.1074
Largest diff. peak and hole	0.338 and -0.351 e.A^{-3}

TABLE-3
SELECTED BOND LENGTHS (Å) OF ENMB-Mn COMPLEX

Mn1-O2	2.1347 (12)	C10-C9	1.482 (2)
Mn1-N1	2.3728 (14)	C11-C12	1.381 (3)
Mn1-N1	2.3728(14)	C15-C14	1.386 (3)
Mn1-Cl1	2.4967 (4)	C8-C5	1.452 (2)
Mn1-Cl1	2.4967 (4)	C7-C2	1.379 (3)
N1-C8	1.279 (2)	C7-C6	1.380 (3)
N1-N2	1.3889 (18)	C5-C6	1.384 (2)
O2-C9	1.241 (2)	C5-C4	1.396 (2)
O1-C2	1.359 (2)	C2-C3	1.385 (3)
O1-C1	1.413 (3)	C4-C3	1.368 (3)
N2-C9	1.340 (2)	C14-C13	1.375 (3)
C10-C15	1.385 (2)	C13-C12	1.371 (3)
C10-C11	1.389 (2)	–	–

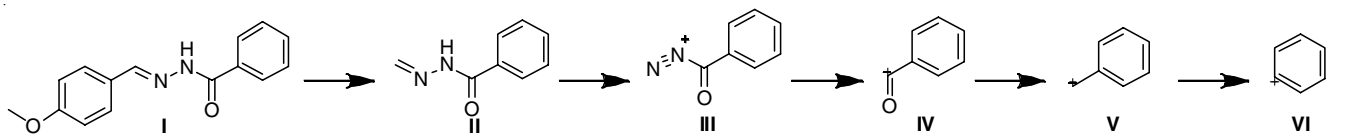

Scheme-III: Mass fragmentation of ENMB-Mn complex

TABLE-4
BOND ANGLES (°) OF ENMB-Mn COMPLEX

O2-Mn1-O2	180.00(5)	C15-C10-C9	116.91(15)
O2-Mn1-N1	107.92(5)	C11-C10-C9	123.49 (16)
O2-Mn1-N1	72.08(5)	C10-C15-C14	119.78(19)
O2-Mn1-N1	72.08(5)	N1-C8-C5	123.78(16)
O2-Mn1-N1	107.92(5)	N1-C8-H8	121.8(15)
N1-Mn1-N1	180.00(1)	C5-C8-H8	114.5(15)
O2-Mn1-Cl1	90.71(4)	C2-C7-C6	119.95(18)
O2-Mn1-Cl1	89.29(4)	C6-C5-C4	118.24(17)
N1-Mn1-Cl1	87.42(3)	C6-C5-C8	123.06(16)
N1-Mn1-Cl1	92.58(3)	C4-C5-C8	118.67(16)
O2-Mn1-Cl1	89.29(4)	O1-C2-C7	124.34(19)
O2-Mn1-Cl1	90.71(4)	O1-C2-C3	115.82(18)
N1-Mn1-Cl1	92.58(3)	C7-C2-C3	119.82(17)
N1-Mn1-Cl1	87.42(3)	C7-C6-C5	120.95(17)
C8-N1-N2	114.79(14)	O2-C9-N2	121.36(15)
C8-N1-Mn1	138.76(12)	O2-C9-C10	120.40(15)
N2-N1-Mn1	105.48(10)	N2-C9-C10	118.24(15)
C9-O2-Mn1	118.20 (11)	C3-C4-C5	121.01(18)
C2-O1-C1	118.39(18)	C13-C14-C15	120.10(2)
C9-N2-N1	118.60(14)	C4-C3-C2	120.01(18)
C9-N2-H2	127.3(18)	C12 C13 C14	120.41(18)
N1-N2-H2	113.8(18)	C13 C12 C11	120.09(19)

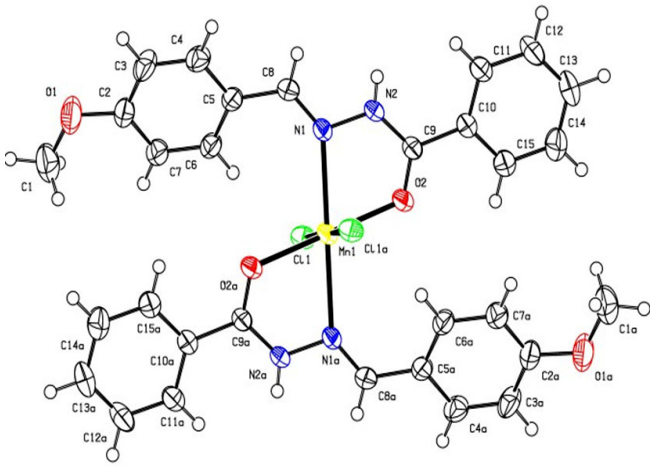

Fig. 3. ORTEP diagram of ENMB-Mn complex

as centro-symmetric system. The structure consists of a unique manganese atom at center surrounded by two chlorine atoms and an independent free two ENMB molecules placed in front positions of central manganese atom. ENMB molecule exists as neutral (act as Lewis base) by coordinate covalent bonds with the central manganese cation (act as Lewis acid) in the complex stable molecule. The hydrogen bonding interactions are listed in Table-5. The two ENMB molecules are interlinked covalently with central manganese atom through nitrogen and oxygen atom with bond length is 2.37 and 2.13 Å, respectively. Further the coordination complex has five intermolecular H-bonding interactions are $C_6H_6\cdots Cl_1$, $N_2H_2\cdots Cl_1$, $C_8H_8\cdots Cl_1$, $C_{11}H_{11}\cdots Cl_1$ and $C_{14}H_{14}\cdots O_1$ and the distance between interaction of donor (hydrogen) and acceptor atom are observed 2.72, 2.45, 2.76, 2.68 and 2.53 Å, respectively. Mn(II) is in a slightly distorted octahedral environment, which is connected to one nitrogen atoms N1, one oxygen atom O1 from two chelating bidentate Schiff base ligand ENMB and two unidendate chlorine

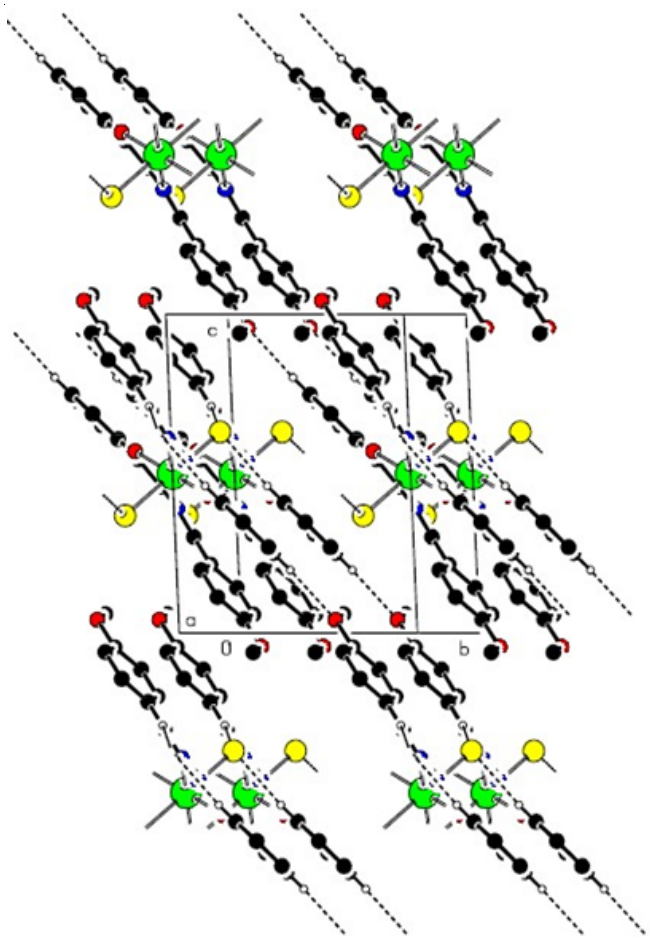

Fig. 4. Packing of ENMB-Mn complex viewed down 'a' axis. Hydrogen bonds are shown as dashed lines

TABLE-5
HYDROGEN BOND DATA (Å) OF
THE COMPOUND (ENMB-Mn)

D–H···A	D–H	H···A	D···A	DHA
C6-H6...Cl1	0.93(1)	2.72(2)	3.6389(19)	171.4(2)
N2-H2...Cl1^{i}	0.80(3)	2.45(3)	3.2380(15)	169.0(2)
C8-H8...Cl1^{i}	0.87(2)	2.76(2)	3.5260(18)	148.0(2)
C11-H11...Cl1^{i}	0.93(1)	2.68(2)	3.606(2)	172.5(2)
C14-H14...O1^{ii}	0.93(1)	2.53(2)	3.453(3)	174.7(2)

Symmetry elements: (i) X+1, Y, Z (ii) X, Y+1, Z-1

atoms. Therefore, conclusion is that the ligand ENMB have neutral bidentate nature and it coordinate through N and O of ENMB to Mn(II) ions.

Thermal studies: In TGA analysis, the rate of heating was maintained at 15 ºC min^{-1} under inert atmosphere. The weight loss was measured from room temperature to 900 ºC. The ENMB-Mn complex has been degradation into three steps. The first step is removal of water molecule of ENMB-Mn from temperature 150 ºC to 300 ºC, which is 10% (Fig. 5). Second step involves maximum (50%) weight loss indicates that removal of all organic moieties like ENMB ligand in temperature range from 300 ºC to 600 ºC. The third step shows the 30% weight loss corresponding to elimination of chlorine ligand in between temperature range from 650 ºC to 750 ºC. Finally, the residue was estimated as pure MnO at above 750 ºC [45-48].

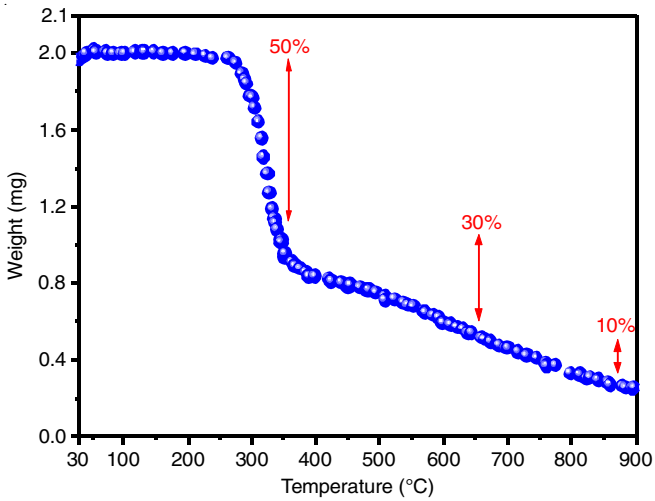

Fig. 5. TGA curve of ENMB-Mn complex

Hirshfeld surface studies: Hirshfeld 3D surfaces of d_{norm}, d_i, d_e, shape index curveness for ENMB-Mn compound are shown in Fig. 6. Mapping of d_{norm} over the Hirshfeld surface in the range –0.7681 to 1.4425 is shown in Fig. 6c. It shows the intermolecular interactions with the adjacent molecules. The d_{norm} map values over the Hirshfeld surface, are shown by a red-white-blue colour pattern. These coloured regions have specific indicative meaning.

The red region indicates that the closer contacts with negative d_{norm} value. White region indicates that contact at van der Waals separation with zero value. While the blue region indicates that the longer contacts with positive d_{norm} value. In ENMB-Mn crystal, the huge circular red patches on d_{norm} surfaces suggests the hydrogen bonding while other patches suggests the oxygen bonded with other atoms. Further, the red and blue areas indication of the negative and positive electrostatic potentials, respectively. This electrostatic potentials related to the acceptor and donor atoms in the interactions during crystal formations [49].

Shape index on the Hirshfeld surface can be used to find interpretation of π-π stacking. Neighboring red and blue triangles are observed in present ENMB-Mn crystal surfaces, which suggest that π-π interaction is observed. UV-Visible spectrum results also agreement to each other. Hollow region indicated by red patches and bump region indicated by blue patches *via* these molecular surfaces touches each other [50,51].

The construction of two-dimensional fingerprint graphs are carried by collecting (d_i, d_e) pairs. The corresponding 2-D fingerprint plots for Hirshfeld surfaces of the ENMB-Mn molecule showing significant intermolecular interactions. The percentage of involvements of various bonding to the total Hirshfeld surface area are given in Fig. 7. It is observed that H···H interactions in ENMB-Mn molecule, which is a notable contribution among all the total Hirshfeld surfaces. This clearly replicating

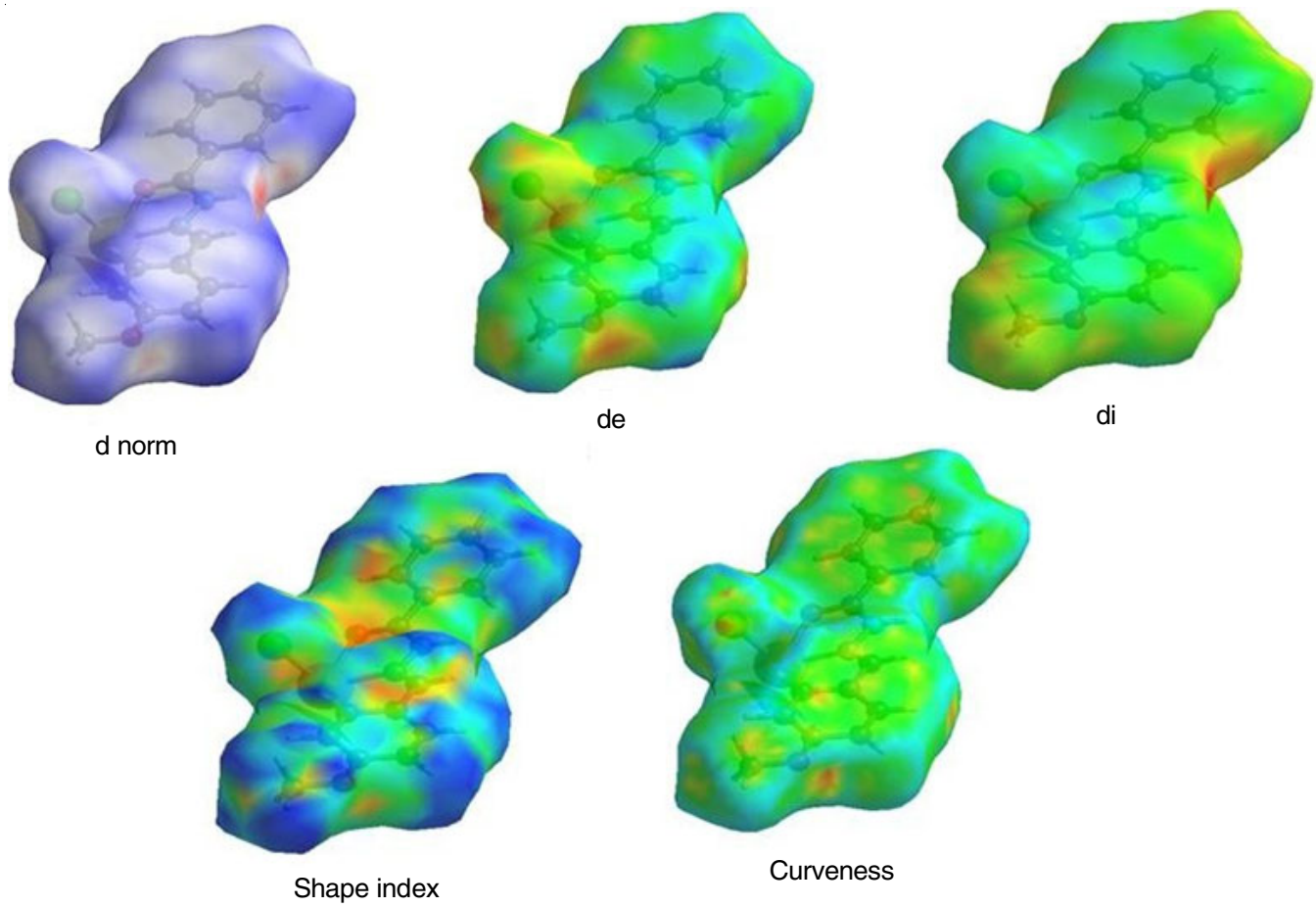

Fig. 6. 3D-Hirshfeld images d norm, de, di, shape index, curvedness ENMB-Mn complex

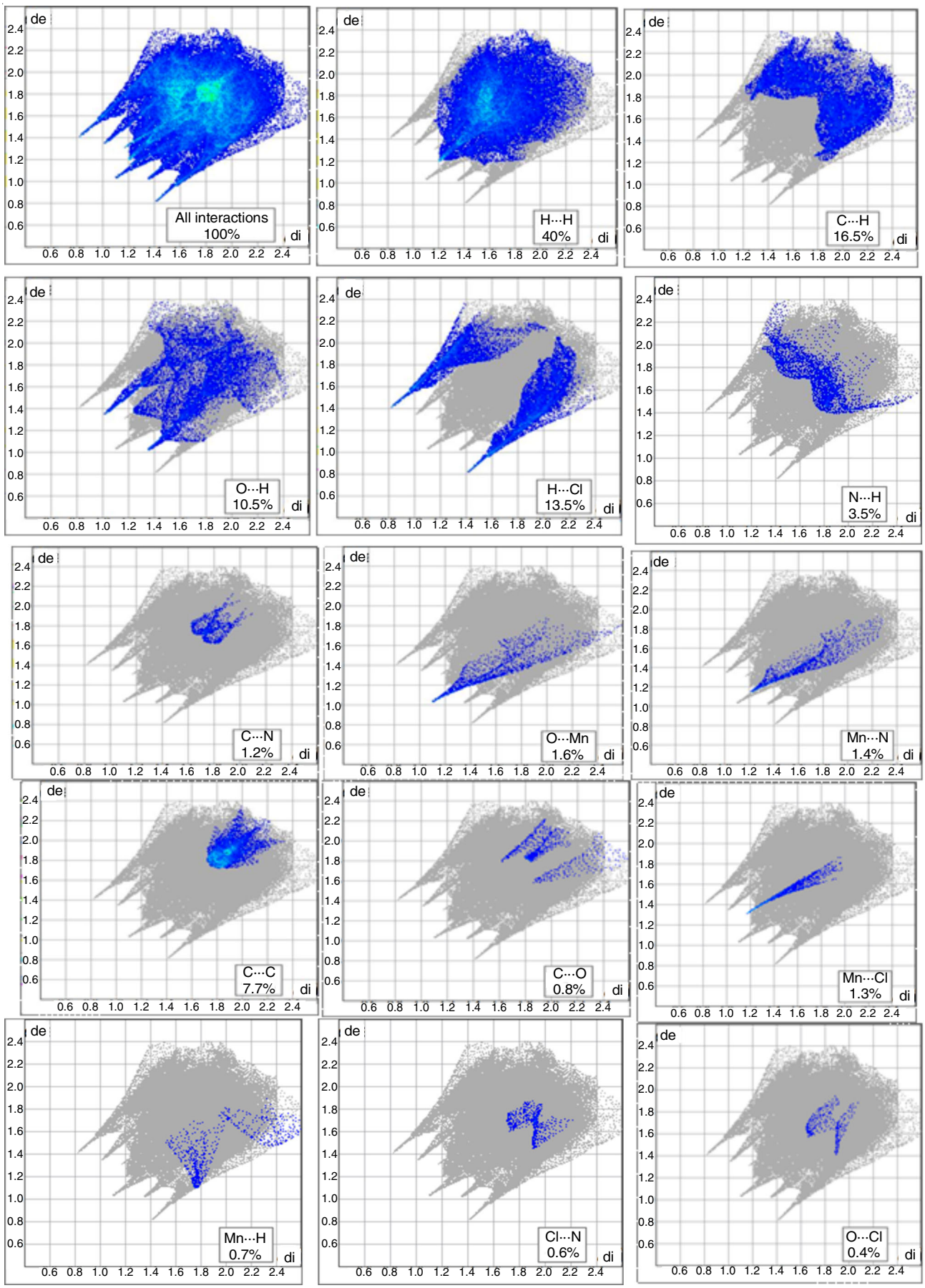

Fig. 7. 2D Hirshfeld fingerprint images of ENMB-Mn complex for all elements

that focus of scattered points in the 2-D fingerprint plot is H···H interaction. These graphs indicates the involvements of selected some intermolecular contacts to the Hirshfeld surfaces. The all interactions in percentage for ENMB-Mn complex showing H···H, C···H, O···H, H···Cl, N···H, C···N, O···Mn, Mn···N, C···C, C···O, Mn···Cl, Mn···H, Cl···N and O···Cl are 100, 40, 16.5,10.5,13.5, 3.5, 1.2, 1.6, 1.4 , 7.7 ,0.8, 1.3, 0.7, 0.6 and 0.4, respectively.

Conclusion

In the present study, novel ENMB-Mn complex of the ligand, dichlorodi(*E*)-*N*′-(4-methoxybenzylidene)benzohydrazide (ENMB) with Mn(II)ion was synthesized. The molecular structures of ligand and manganese complex were confirmed by spectroscopic techniques. The single crystal XRD analysis of ENMB-Mn indicates that crystal structure is to be triclinic with space group P-1, the structure is complete octahedral geometry and the ratio of manganese(II) ion, ENMB and chlorine ratio is 1:2:2, respectively. Thermal behaviour of ENMB-Mn shows that the crystal can withstand at high temperature. Hirshfeld surface study clearly supports the maximum crystal voids are present since packing density is half than total volume of unit cell of title crystal compound, which is helpful for charge transfer and it will be used as a non-linear optical materials.

CONFLICT OF INTEREST

The authors declare that there is no conflict of interests regarding the publication of this article.

REFERENCES

1. G.G. Mohamed, M.A. Zayed and S.M. Abdallah, *J. Mol. Struct.*, **62**, 979 (2010); https://doi.org/10.1016/j.molstruc.2010.06.002
2. C. Maxim, T.D. Pasatoiu, V.C. Kravtsov, S. Shova, C.A. Muryn, R.E.P. Winpenny, F. Tuna and M. Andruh, *Inorg. Chim. Acta*, **361**, 3903 (2008); https://doi.org/10.1016/j.ica.2008.03.013
3. S. Nayak, P. Gamez, B. Kozlevèar, A. Pevec, O. Roubeau, S. Dehnen and J. Reedijk, *Polyhedron*, **29**, 2291 (2010); https://doi.org/10.1016/j.poly.2010.04.035
4. M. Yuan, F. Zhao, W. Zhang, Z.M. Wang and S. Gao, *Inorg. Chem.*, **46**, 11235 (2007); https://doi.org/10.1021/ic701655w
5. S. Triki, C.J. Gomez-Garcia, E. Ruiz and J. Sala-Pala, *Inorg. Chem.*, **44**, 5501 (2005); https://doi.org/10.1021/ic0504543
6. J. Ribas, A. Escuer, M. Monfort, R. Vicente, R. Cortes, L. Lezama and T. Rojo, *Coord. Chem. Rev.*, **193-195**, 1027 (1999); https://doi.org/10.1016/S0010-8545(99)00051-X
7. J. S. Miller and M. Drillon, Magnetism: Molecules to Materials I: Models and Experiments, Wiley-VCH Verlag GmbH (2002).
8. S. Banerjee, A. Ray, S. Sen, S. Mitra, D.L. Hughes, R.J. Butcher, S.R. Batten and D.R. Turner, *Inorg. Chim. Acta*, **361**, 2692 (2008); https://doi.org/10.1016/j.ica.2008.01.019
9. S. Banerjee, S. Sen, S. Basak, S. Mitra, D.L. Hughes and C. Desplanches, *Inorg. Chim. Acta*, **361**, 2707 (2008); https://doi.org/10.1016/j.ica.2008.01.020
10. A.M. Stadler and J. Harrowfield, *Inorg. Chim. Acta*, **362**, 4298 (2009); https://doi.org/10.1016/j.ica.2009.05.062
11. B. Shaabani, A.A. Khandar, N. Ramazani, M. Fleck, H. Mobaiyen and L. Cunha-Silva, *J. Coord. Chem*., **70**, 696 (2017); https://doi.org/10.1080/00958972.2016.1274028
12. S. Banerjee, S. Mondal, W. Chakraborty, S. Sen, R. Gachhui, R.J. Butcher, A.M.Z. Slawin, C. Mandal and S. Mitra, *Polyhedron*, **28**, 2785 (2009); https://doi.org/10.1016/j.poly.2009.05.071
13. G.F. de Sousa, C.A.L. Filgueiras, A. Abras, S.S. Al-Juaid, P.B. Hitchcock and J.F. Nixon, *Inorg. Chim. Acta*, **218**, 139 (1994); https://doi.org/10.1016/0020-1693(94)03798-1
14. S. Seth and S. Chakraborty, *Acta Crystallogr. C*, **40**, 1530 (1984); https://doi.org/10.1107/S0108270184008593
15. G. Wang, K. Leus, S. Couck, P. Tack, H. Depauw, Y.-Y. Liu, L. Vincze, J.F.M. Denayer and P. Van Der Voort, *Dalton Trans.*, **45**, 9485 (2016); https://doi.org/10.1039/C6DT01355D
16. A. Schneemann, V. Bon, I. Schwedler, I. Senkovska, S. Kaskel and R.A. Fischer, *Chem. Soc. Rev.*, **43**, 6062 (2014); https://doi.org/10.1039/C4CS00101J
17. C.R. Murdock, B.C. Hughes, Z. Lu and D.M. Jenkins, *Coord. Chem. Rev.*, **258-259**, 119 (2014); https://doi.org/10.1016/j.ccr.2013.09.006
18. Z.J. Lin, J. Lu, M. Hong and R. Cao, *Chem. Soc. Rev.*, **43**, 5867 (2014); https://doi.org/10.1039/C3CS60483G
19. Y. Takashima, V.M. Martinez, S. Furukawa, M. Kondo, S. Shimomura, H. Uehara, M. Nakahama, K. Sugimoto and S. Kitagawa, *Nat. Commun.*, **2**, 1 (2011); https://doi.org/10.1038/ncomms1170
20. R.M.P. Colodrero, P. Olivera-Pastor, E.R. Losilla, M.A.G. Aranda, L. Leon-Reina, M. Papadaki, A.C. McKinlay, R.E. Morris, K.D. Demadis and A. Cabeza, *Dalton Trans.*, **41**, 4045 (2012); https://doi.org/10.1039/c2dt11992g
21. M.M.E. Shakdofa, M.H. Shtaiwi, N. Morsy and T.M.A. Abdel-Rassel, *Main Group Chem.*, **13**, 187 (2014); https://doi.org/10.3233/MGC-140133
22. O. Pouralimardan, A.C. Chamayou, C. Janiak and H.H. Monfared, *Inorg. Chim. Acta*, **360**, 1599 (2007); https://doi.org/10.1016/j.ica.2006.08.056
23. S. Rathi, A. Maji, U.P. Singh and K. Ghosh, *Inorg. Chim. Acta*, **486**, 261 (2019); https://doi.org/10.1016/j.ica.2018.09.081
24. A. Banerjee, A.S. Tolla, S. Stjepanovic, M.D. Sevilla, J.L. Goodsell, A. Angerhofer, W.W. Brennessel, R. Loloee and F.A. Chavez, *Inorg. Chim. Acta*, **486**, 546 (2019); https://doi.org/10.1016/j.ica.2018.11.013
25. J.P. Zhang, P.Q. Liao, H.L. Zhou, R.B. Lin and X.M. Chen, *Chem. Soc. Rev.*, **43**, 5789 (2014); https://doi.org/10.1039/C4CS00129J
26. J.J.R. Frasto da Silva and R.J.P. Williams, The Biological Chemistry of the Elements, Clarendon Press: Oxford (1994).
27. P.M. Cullis, eds.: Acyl Group Transfer-Phosphoryl Transfer, In: Enzyme Mechanisms, Royal Society of Chemistry, London, pp. 179-220 (1987).
28. Y. Tang, J. Li and J. Zhang, *Prog. React. Kinet. Mech.*, **34**, 373 (2009); https://doi.org/10.3184/146867809X466816
29. B. Shaabani, A.A. Khandar, N. Ramazani, M. Fleck, H. Mobaiyen and L. Cunha-Silva, *J. Coord. Chem.*, **70**, 696 (2017); https://doi.org/10.1080/00958972.2016.1274028
30. M. Boutar, C. Desroches, N. Mattoussi, M. Habib Noamane, L. Bois, I. Gautier-Luneau, R. Abidi and D. Luneau, *Inorg. Chim. Acta*, **486**, 562 (2019); https://doi.org/10.1016/j.ica.2018.11.001
31. S. Wolff, D. Grimwood, J. McKinnon, M. Turner, D. Jayatilaka and M. Spackman, Crystal Explorer, University of Western Australia (2012).
32. R.M. Silverstein, F.X. Webster and D.J. Kiemle, Spectrometric Identification of Organic Compounds, Wiley & Sons, Inc., edn 7 (2005)
33. N.P.G. Roeges, A Guide to Complete Interpretation of IR Spectra of Organic Structures, New York: Wiley (1994).
34. R.V. Singh, N. Fahmi and M.K. Biyala, *J. Iran. Chem. Soc.*, **2**, 40 (2005); https://doi.org/10.1007/BF03245778
35. I.O. Adeoye, O.O. Adelowo, M.A. Oladip and O.A. Odunola, *Res. J. Appl. Sci.*, **2**, 590 (2007).
36. Z. Dori, R.F. Ziolo, A.P. Gaughan, C.G. Pierpont and R. Eisenberg, *Inorg. Chem.*, **10**, 1289 (1971); https://doi.org/10.1021/ic50100a038
37. S.B. Baul, T.S.B. Baul and E. Rivarola, *Synth. React. Inorg. Met.-Org. Chem.*, **29**, 215 (1999); https://doi.org/10.1080/00945719909349445
38. P. Drozdzewski, A. Brozyna, M. Kubiak and T. Lis, *Vib. Spectrosc.*, **40**, 118 (2006); https://doi.org/10.1016/j.vibspec.2005.07.007

39. M.C. Sharma, N.K. Sahu, D.V. Kohli, S.C. Chaturvedi and S. Sharma and *J. Dig. Nanomat. Biostruct.*, **4**, 361 (2009).
40. P. Kumar, B. Narasimhan and D. Sharma, *ARKIVOC*, 159 (2008); https://doi.org/10.3998/ark.5550190.0009.d19
41. O. Tamer, D. Avcý and Y. Atalay, *J. Phys. Chem. Solids*, **99**, 124 (2016); https://doi.org/10.1016/j.jpcs.2016.08.013
42. S. Altürk, D. Avcý, Ö. Tamer, Y. Atalay and O. Sahin, *J. Phys. Chem. Solids*, **98**, 71 (2016); https://doi.org/10.1016/j.jpcs.2016.06.008
43. H.Z. Chohan and M. Praveen, *Pak. J. Pharm. Sci.*, **12**, 1 (1999).
44. F.X. Webster and D.J. Kiemle, ed.: R.M. Silverstein, Spectrometric Identification of Organic Compounds, John Wiley & Sons, Inc. (2005).
45. S.I. Mostafa, *Transition Met. Chem.*, **32**, 769 (2007); https://doi.org/10.1007/s11243-007-0247-x
46. S.A. Elsayed, A.M. El-Hendawy, S.I. Mostafa, B.J. Jean-Claude, M. Todorova and I.S. Butler, *Bioinorg. Chem. Appl.*, **2010**, 149149 (2010); https://doi.org/10.1155/2010/149149
47. S.I. Mostafa, C. Papatriantafyllopoulou, S.P. Perlepes and N. Hadjiliadis, *Bioinorg. Chem. Appl.*, **2008**, 647873 (2008); https://doi.org/10.1155/2008/647873
48. Themed Collection: Structural Design of Coordination Polymers, RSC papers, pp. 1-10.
49. J.J. McKinnon, A.S. Mitchell and M.A. Spackman, *Chem. Eur. J.*, **4**, 2136 (1998); https://doi.org/10.1002/(SICI)1521-3765(19981102)4:11<2136::AID-CHEM2136>3.0.CO;2-G
50. M.A. Spackman and D. Jayatilaka, *CrystEngComm*, **11**, 19 (2009); https://doi.org/10.1039/B818330A
51. R. Hoffmann, Solids and Surfaces: A Chemist's View of Bonding in Extended Structures,VCH Publishers: New York (1988).